Draft version October 4, 2020
Typeset using LaTeX default style in AASTeX62

Placing Empirical Constraints on CCSNe Yields using VMP DLA's

Evan H. Nuñez[1] and Evan N. Kirby[1]

[1] *California Institute of Technology, 1200 E. California Blvd., MC 249-17, Pasadena, CA 91125, USA*

ABSTRACT

I place empirical constraints on the core collapse supernovae (CCSNe) yields of zero-metallicity massive stars using the abundances measured in very metal-poor (VMP; [Fe/H] < -2) Damped Lyman Alpha Absorbers (DLAs). I first compile a high quality, high volume sample of VMP DLAs by reviewing more than 30 years of literature. With the reliable sample I plot the abundance ratios of C, N, O, Al, Si, and S as a function of Fe to find their averages, which gives the empirical CCSNe abundance ratio for that element. I convert these abundance ratios into absolute abundances, and compare them to theoretical yields. I find that differences range from <0.2 dex (Si and S) at best, up to 1.7 dex (N) at worst. Finally, I run a galactic chemical evolution model to compare the predicted abundance ratios of the dwarf galaxy Sculptor using standard theoretical yields and VMP DLA constrained yields. I find differences ≤0.3 dex, for all elements at the lowest metallicities, [Fe/H] < -2, and find little to no difference at the highest metallicities, [Fe/H] > -1.5, where Type Ia supernovae dominate the chemical evolution rather than CCSNe. Next steps would be to compare more yield tables, apply them to GCE models that have a Markov-Chain Monte-Carlo framework attached to it, and acquire more VMP DLA data.

1. INTRODUCTION

1.1. *Core Collapse Supernovae*

Core Collapse Supernovae (CCSNe) play a vital role in the evolution of the universe. They drive, and/or substantially contribute to, many astrophysical processes including the creation of heavy metals, injection of both heavy metals and large amounts of energy into the interstellar medium, and the chemical evolution of galaxies and more (Woosley et al. 2002; Pettini 2011). Since the timescales associated with CCSNe are so short, astronomically speaking, it is difficult to place observational constraints on the yields from zero-metallicity stars such that if one wants to predict the yields of these CCSNe they must model the nonlinear physics of stellar nucleosynthesis.

Modeling the yields of CCSNe is a challenge that is fraught with many uncertainties (Woosley & Weaver 1995; Heger & Woosley 2010; Nomoto et al. 2006; Romano et al. 2010). These uncertainties compound with one another, in ways that can drastically affect the resulting yield prediction. These uncertainties include, but are not limited to, the pre-supernova evolution of the star, the nuclear reaction rates that are adopted for each reaction, the explosion mechanism, and the explosion energy (Woosley & Weaver 1995; Nomoto et al. 2006; Romano et al. 2010). One can see how these can compound since the nuclear reaction rates would sensitively affect the pre-supernova evolution of the star as well as the explosive nucleosynthesis, the pre-supernova evolution of the star fundamentally changes the structure of the star which then affects the explosion mechanism (i.e., mass piston or thermal bomb Woosley & Weaver 1995). Additionally, the theory that is used to describe a physical process could affect the results such as what theory of convection is adopted (i.e., Schwarzschild or Ledoux criterion Woosley & Weaver 1995; Woosley et al. 2002; Romano et al. 2010). All of these effects combine to either skew the resulting modeled yields to either under-represent or over-represent that one would observes in nature.

One application that CCSNe yields play a critical role in is the modeling galactic chemical evolution (GCE). These models track the abundances of elements over the history of a galaxy. These models can take many forms, from the physics rich simulations Hopkins et al. (i.e., FIRE-2 2018) to simpler one-zone models Côté et al. (i.e., OMEGA 2016). Even though the models can range tremendously in their physical diversity, they are fundamentally rely on theoretical

Corresponding author: Evan Haze Nuñez
enunez@astro.caltech.edu

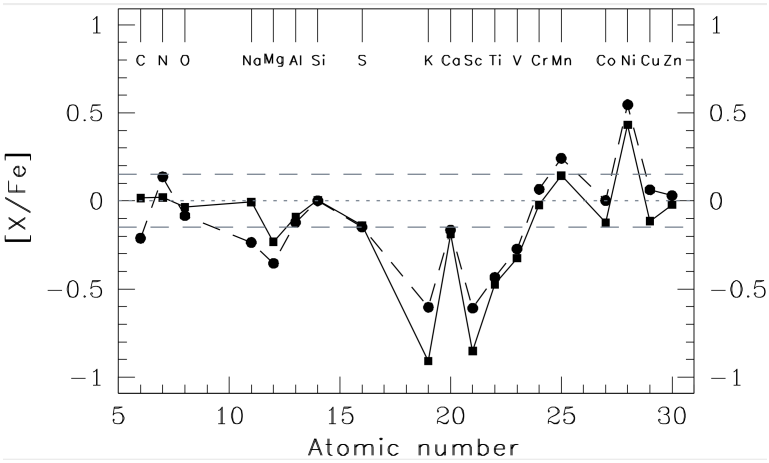

Figure 1. Figure 23 from Romano et al. (2010). Predicted abundance ratios using the two-infall GCE model of the Milky Way from Chiappini et al. (1997); Chiappini (2001) at the Sun's birth with all parameters held constant except the adopted yields. Model 1, black dashed lines and circles use Case A of the CCSNe yields from (Woosley & Weaver 1995). Model 2, solid lines and squares, uses Case B from Woosley & Weaver (1995).

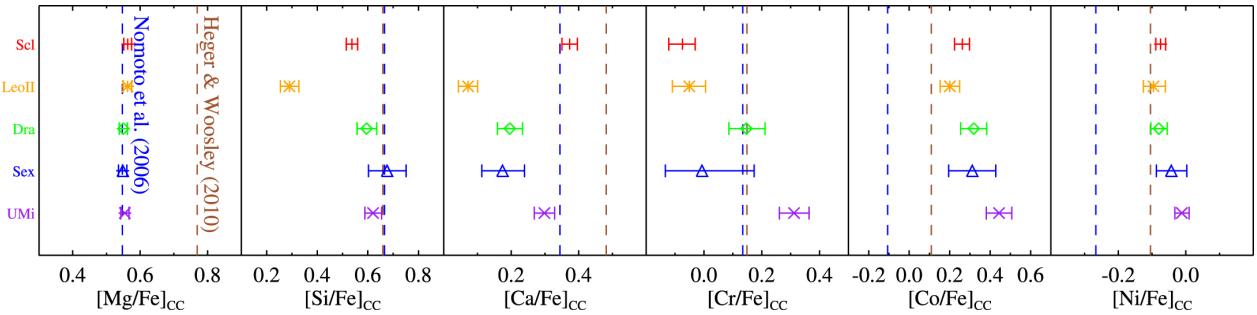

Figure 2. Figure 7 from Kirby et al. (2019). Empirical placements on CCSNe yields using metal-poor stars in the dwarf galaxies Sculptor, Leo II, Draco, Sextans, and Ursa Minor compared to theoretical yields from Nomoto et al. (2006) and Heger & Woosley (2010). The colored shapes are the empirical yields inferred from the dwarf galaxies and the dashed lines are from the theoretical yields.

stellar yields to inform how CCSNe would enrich the gas reservoir. As mentioned previously, there can be tremendous diversity between different theoretical yields and their affects can be seen in Figure 1 from Romano et al. (2010, R10).

R10 used a GCE model to predict the abundance ratios of a Milky Way like galaxy at the Sun's birth for C to Zn (Figure 1). R10 held everything about the models constant except the yields that were adopted. The difference between the CCSNe yields that were adopted are their explosion energy (Model 1 being 1.2 x 10^{51} and Model 2 being 1.9 x 10^{51} erg) which are Case A and Case B models from Woosley & Weaver (1995). The result shows that the predictions differ enough that for any given element, it is possible that one of the models will be inside of the acceptable tolerances (dashed horizontal lines in Figure 1) and the other will not.

1.2. *Using Stars to Constrain CCSNe Yields*

Metal-poor stars in the galactic halo and dwarf galaxies are Population II stars that condensed from gas that was near primordial. This means that the abundances in the atmospheres of these stars should be reflective of the near primordial gas which had to have been enriched primarily by CCSNe. This method has been used to place empirical constraints on CCSNe. The most recent example is from Kirby et al. (2019); de los Reyes et al. (2020) shown in Figure 2.

Once can see that there can be differences of up to 0.3 dex between at least one of the empirical yields and one theoretical prediction. The difficulty with placing constraints using stars is that their abundances could have large uncertainties due to non Thermodynamic Equilibrium (nLTE) effects for some lines. This means that not all of the measurements of abundances from stars are trustworthy and/or truly reflective of the gas that they condensed from.

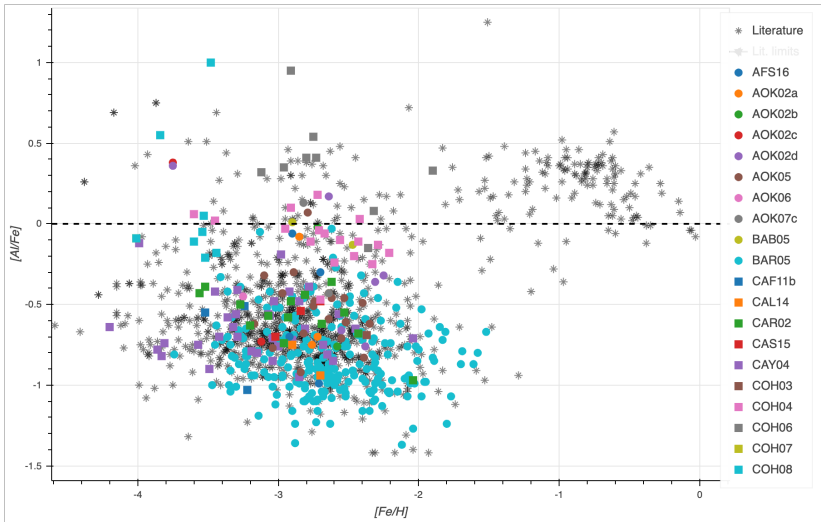

Figure 3. Al abundance ratios of metal-poor stars from the galactic halo, stellar bulge, and dwarf galaxies compiled in the JINAbase database (Abohalima & Frebel 2018). The clusters at the bottom left and top right arise from the differnt lines that were used to measure the abundances, 396 nm singlet and 670 nm doublet respectively. The discrepancies in their abundances are a result of nLTE affects in the 396 nm singlet.

The most egregious example of this, and a true cautionary tale, can be seen in Figure 3 which plots the Al abundances ratio as a function of Fe.

There are two distinct clusters that are formed in what looks like a messy scatter plot. The clusters arise from the two different lines that are used to measure the abundance of Al. The cluster on the lower left, centered around [Fe/H] $\sim$ -3 and [Al/Fe] $<$ solar, uses the Al 396 nm singlet whereas the cluster on the top right, centered around [Fe/H] $\sim$ -1 and [Al/Fe] $>$ solar, uses the Al 670 nm doublet. The 670 nm doublet is a weak line that is generally difficult to measure unless at higher metallicities whereas the 396 nm singlet is a strong line that is used when the 670 nm singlet is unavailable, which occurs at low metallicities. The discrepancy between the abundances, $>$ 0.6 dex, can be traced to nLTE effects present in the 396 nm singlet.

Stars act as a middle-man to the abundances from near primordial gas which, as shown, can be problematic. But there exists objects that allow us to probe this same gas without the complication of a stellar atmosphere.

1.3. *Very Metal-Poor Damped Lyman Alpha Absorbers*

Very Metal-Poor (VMP) Damped Lyman Alpha Absorbers (DLA) offer a unique way to investigate nearly primordial gas without the need of stars, which are fraught with large and uncertain nLTE effects. VMP DLAs are effectively the gas that Population II stars condensed from so measuring their abundances is measuring the near primordial gas.

VMP DLAs are a class of QSO absorber classified by their large column density $N_H > 2 \times 10^{20} cm^{-2}$ and large damped absorption of the Lyman-alpha emission line, as example of which is shown in Figure 4. They are large reservoirs of neutral hydrogen that lie at high redshift (z $\sim$ 3). They make up around $\sim$90% of the neutral hydrogen content in the universe at their redshift (Pettini 2011; Cooke & Madau 2014).

VMP DLAs are ideal for the following reasons 1) Their metal-poor status mean that they have seen only few enrichment events in their history, 2) since they lie at such high redshift, their enrichment would have to have come from primarily CCSNe since there would have been enough time for delayed enriching events to have occurred (i.e., Type Ia supernovae (SNe Ia) or winds from AGB stars), and 3) measuring abundances from their cool, diffuse gas is straightforward compared to the complications that would arise from a stellar atmosphere.

The goal of this project is to use the abundances measured from VMP DLA's to place empirical constraints on the yields of CCSNe by finding the average of their abundance ratios across -4 $<$ [Fe/H] $<$ -2 then using these constraints to quantify the differences between theoretical yields and their evolution through a GCE model. In Section 2 I discuss how I compiled my sample of VMP DLA's and discuss considerations that arise in the determination of their abundances. In Section 3 I estimate the empirical CCSNe abundance ratios for C, N, O, Al, Si, and S by plotting the abundance ratios of VMP DLA's as a function of Fe then calculating the linear average. In Section 4 I convert the constraints

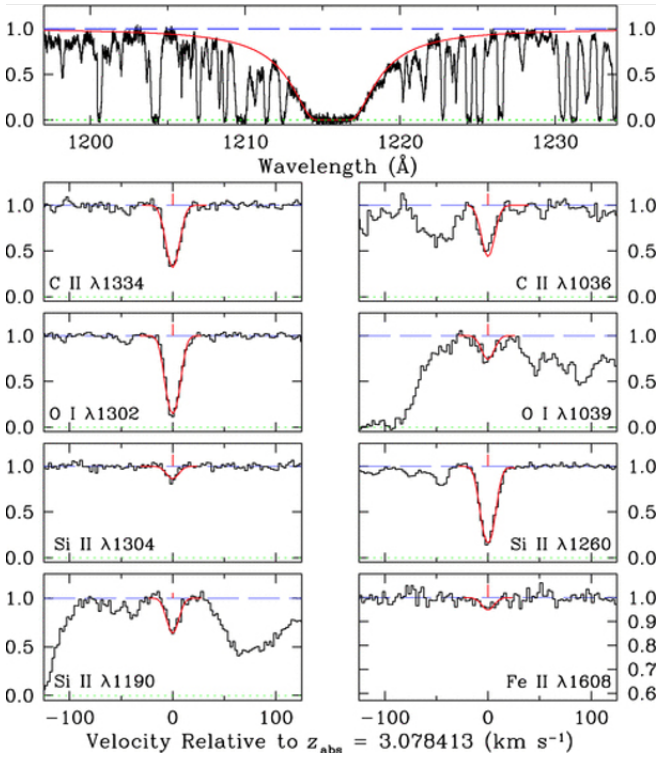

Figure 4. Figure 3 of Cooke et al. (2011b), showing the high-resolution spectra of the VMP DLA towards QSO J1001+0343.

of the ratios to constraints on the elemental yields, then compare the constraints to theoretical yields and a galactic chemical evolution model. In Section 5 I discuss next steps for the project.

2. SAMPLE SELECTION

My sample is built from a review of more than 30 years of literature. I came across four different surveys over three different decades, and around 50 papers detailing both the surveys and individual sources.

2.1. *Observations*

I will summarize the broad observational strategies conducted across the various datasets that I compiled. The majority of sources in my sample have high-resolution spectroscopic measurements. The observations were mainly split between the High Resolution Echelle Spectrometer (HIRES) (Vogt et al. 1994) on Keck I at Keck Observatory, and the Ultraviolet and Visual Echelle Spectrograph (UVES) (Dekker et al. 2000) on the Very Large Telescope (VLT) at the European Southern Observatory. HIRES covers a spectral range of 4000-8000 Å between its two blue and red configurations in the observers frame with a resolution R > 30,000. UVES has a spectral range of 3000-8000 Å between ita red and blue configuration with a spectral resolution of R $\geq 40,000$.

In my compilation there are a handful of sources that were obtained using the Echelle Spectrometer and Imager (ESI) (Sheinis et al. 2002) on Keck II . ESI spans a spectral range of 3900-10900 Å and has a resolution R $\geq$ 10,000.

The majority of the candidates in my sample have made several iterations through different surveys. The first DLA survey was conducted in 1986 by Wolfe et al. (1986) where they compiled QSO candidates from the literature and followed them up at Lick Observatory. These sources, among others, were subsequently followed up by several authors once HIRES was commissioned in 1994 (i.e., Lu et al. 1998; Prochaska et al. 2001; Prochaska & Wolfe 2002). Even more were followed up, and discovered, following the commissioning of UVES in 2000 (i.e., Molaro et al. 2000; Ellison & Lopez 2001; Molaro et al. 2001; Dessauges-Zavadsky et al. 2001; Levshakov et al. 2002; Lopez et al. 2002; Pettini et al. 2002; Centurión et al. 2003; Dessauges-Zavadsky et al. 2003).

In 2000 the Sloan Digital Sky Survey (SDSS) began operation and its first QSO sample target list was released by (Richards et al. 2002). These sources were later followed up by SDSS low resolution spectroscopy allowing an easy and automated way to search for VMP DLAs. VMP DLA candidates can be found via SDSS selection requiring that only

3 metal lines are observed (Cooke et al. 2011b). The other surveys that made it into my sample include UCSD HIRES DLA Survey (Prochaska et al. 2007), Keck ESI MP DLA Survey (Penprase et al. 2010), and ESO UVES QSO Survey (Zafar et al. 2014). The rest of the sources are compiled from the following papers (Pettini et al. 2008; Petitjean et al. 2008; Ellison et al. 2010; Srianand et al. 2010; Cooke et al. 2011b,a, 2012, 2013; Cooke & Madau 2014; Cooke et al. 2015; Berg et al. 2016; Cooke et al. 2017; D'Odorico et al. 2018; Welsh et al. 2019, 2020).

There are three selection criteria for sources to make it to my final sample; 1) At least a medium resolution spectroscopic measurement, 2) [Fe/H] < -2, and 3) upper and lower bounds on measurements. My final sample contains more than 110 high quality VMP DLAs.

2.2. *Abundance Determinations*

Deriving abundances from VMP DLAs is relatively straightforward compared to stars. One can map directly from equivalent width to column density for all elements of interest. This is primarily due to the fact that there is no need for nLTE corrections for VMP DLAs. Even still, there are other processes that need to be considered when measuring their abundances.

Partial ionization of elements could lead to overestimating, or underestimating, the "true" abundance of a system depending on if the transition measured is the dominant ionization state. This leads to a discrepancy between the "true" abundance and what is measured. In general the ionization corrections for DLAs are low due to their high H I column density which allows the gas to self-shield from the UV background emitting from quasars and galaxies (Wolfe et al. 2005; Pettini 2011). Additionally, it has been shown that in the metallicity range that VMP DLA's reside, [Fe/H] less than 1/100 solar, there is even less need for ionization corrections (Cooke et al. 2011b, 2017). Therefore, partial ionization is not a systemic issue with VMP DLAs.

Dust can lead to underestimating a sources abundance (Wolfe et al. 2005). Refractory elements could condense onto dust grains which removes their signature from the gas phase. This will mean that the abundance measured for an element that suffers from dust depletion would be an underestimate of the "true" abundance. It has been shown that DLAs with [Fe/H] < -2 need little to no dust corrections (Wolfe et al. 2005; Pettini 2011; Cooke et al. 2011b, 2017). Therefore, there is no need to apply dust corrections to my sample.

3. ABUNDANCE RATIOS IN VMP DLAS

Each of the VMP DLAs in our sample have at least three abundance measurements. All sources have two in common, Fe and H. The third varies but is C, N, O, Al, Si, and/or S. After scaling all datasets to the Asplund et al. (2009) solar scale, I plot all of the abundance ratios in my sample as a function of [Fe/H] in Figure 5.

As mentioned previously, there is a delay time between the first enriching events to occur, from CCSNe, and delayed enriching events, i.e., Type Ia SN (SNe Ia) and winds from AGB stars. These processes can be disentangled in the [X/Fe] vs [Fe/H] plots due to [Fe/H] being a rough tracer of age. One expects to see that at the earliest times, or lowest [Fe/H], that the ratios reflect the yields from CCSNe. While at later times, or higher [Fe/H], the ratios reflect a combination of yields from CCSNe and delayed processes.

The former is visually seen as a plateau in [X/Fe] and the latter as a "knee" leading to a steady decline. This is because CCSNe produce both α-elements and Fe-peak elements in roughly the same proportion whereas SNe Ia produce mainly Fe-peak elements and little to no α-elements. Therefore, locating the [X/Fe] plateau gives the abundance ratio of CCSNe.

To obtain where this plateau occurs I take the average of the abundance ratios for each element. An abundance in bracket notation, like [X/Fe], is a logarithmic quantity. However, theoretical supernova yields and chemical evolution models conventionally use linear values. Therefore, I average the abundance ratios in linear space: $\overline{[\mathrm{X/Fe}]} = \log\left(\mathrm{mean}(10^{[\mathrm{X/Fe}]})\right)$. I list the averages in Table 1.

4. YIELD DIFFERENCES

4.1. *Constraining the Yields*

Since I have constraints on ratios but want to constrain the yields for single elements, I must choose an element to scale to. Oxygen generally has the most well understood nucleosynthesis origins as evidenced by the the general agreement that models have with one another regarding their O production and the accuracy of O patterns in GCE models (Woosley & Weaver 1995; Nomoto et al. 2006; Romano et al. 2010). For this reason I use O as the reference "true" element yield.

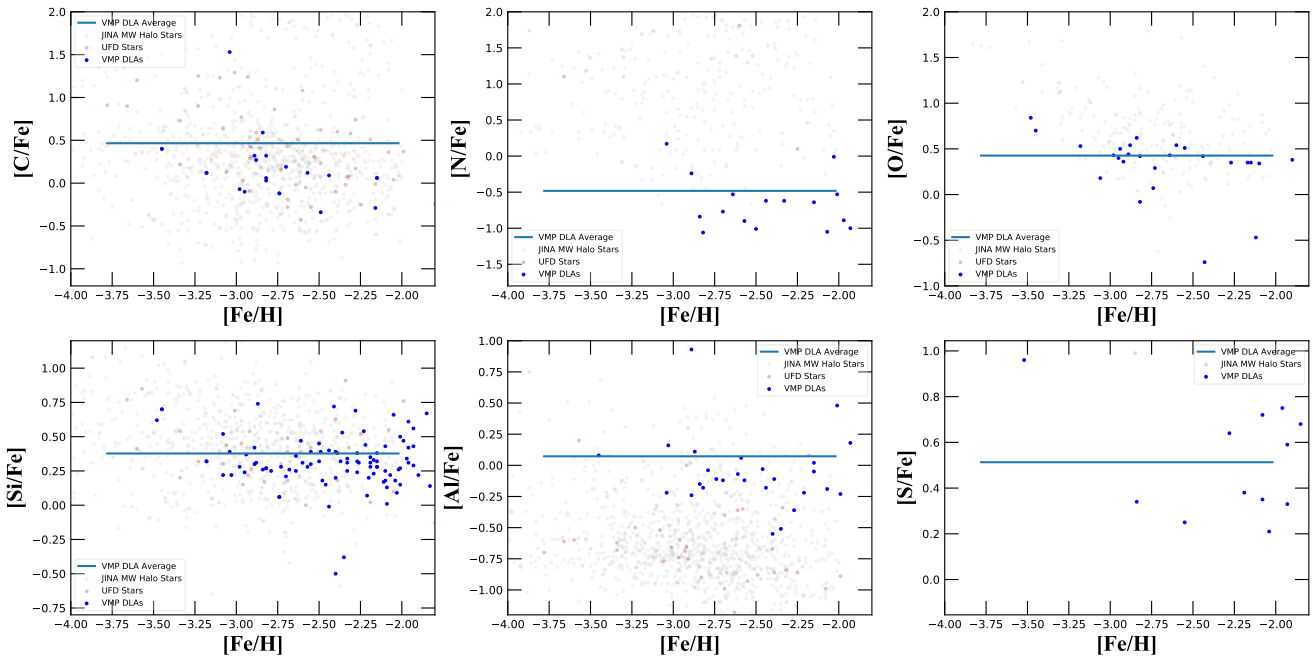

Figure 5. C, N, O, Al, Si, and S abundance ratios as a function of [Fe/H]. The blue large circular points are VMP DLAs. The grey smaller points are metal-poor stars from the JINA database. The red smaller points are from the UFD Star compilation from Alex Ji (references therein). The blue horizontal bar is the logarithm of the linear average of the abundance ratios.

Table 1. $\overline{[X/Fe]}$ of VMP DLAs

Element	$\overline{[X/Fe]}$
C	0.465
N	-0.482
O	0.426
Al	0.0725
Si	0.377
S	0.513

Using O as the reference element I can place constraints on C, N, Al, Si, S, and Fe by converting the abundance ratios to absolute mass ratios and solving for the mass of interest, say element X. This mass though, would be the IMF-averaged mass since the VMP DLAs hold the gas from all enriching events in its enrichment history.

I use the CCSNe yields from Nomoto et al. (2006, hereafter N06) and average their zero-metallicity masses over the Salpeter IMF for the mass range 10 - 100 $M_\odot$ for all elements of interest. The expression to obtain the VMP DLA constrained IMF Averaged Fe yield is shown in Equation 1.

$$\overline{M}_{Fe} = \frac{\overline{M}_O}{10^{(\overline{[O/Fe]}+\log{(n_O)}_\odot-\log{(n_{Fe})}_\odot)}} \frac{m_{Fe}}{m_O} \tag{1}$$

where $\overline{M}_O$ is the IMF-averaged theoretical mass yield of O from N06, $\log{(n_O)}_\odot$ is the solar abundance of Oxygen, $\log{(n_{Fe})}_\odot$ is the solar abundance of Fe, m_{Fe} is the atomic mass of Fe, and m_O is the atomic mass of Oxygen. I can then find that for any general element X, the DLA constrained IMF-averaged mass yield would be given by Equation(s) 2 and 3.

$$\overline{M}_X = \overline{M}_{Fe} * 10^{(\overline{[X/Fe]}+\log{(n_X)}_\odot-\log{(n_{Fe})}_\odot)} \frac{m_X}{m_{Fe}} \tag{2}$$

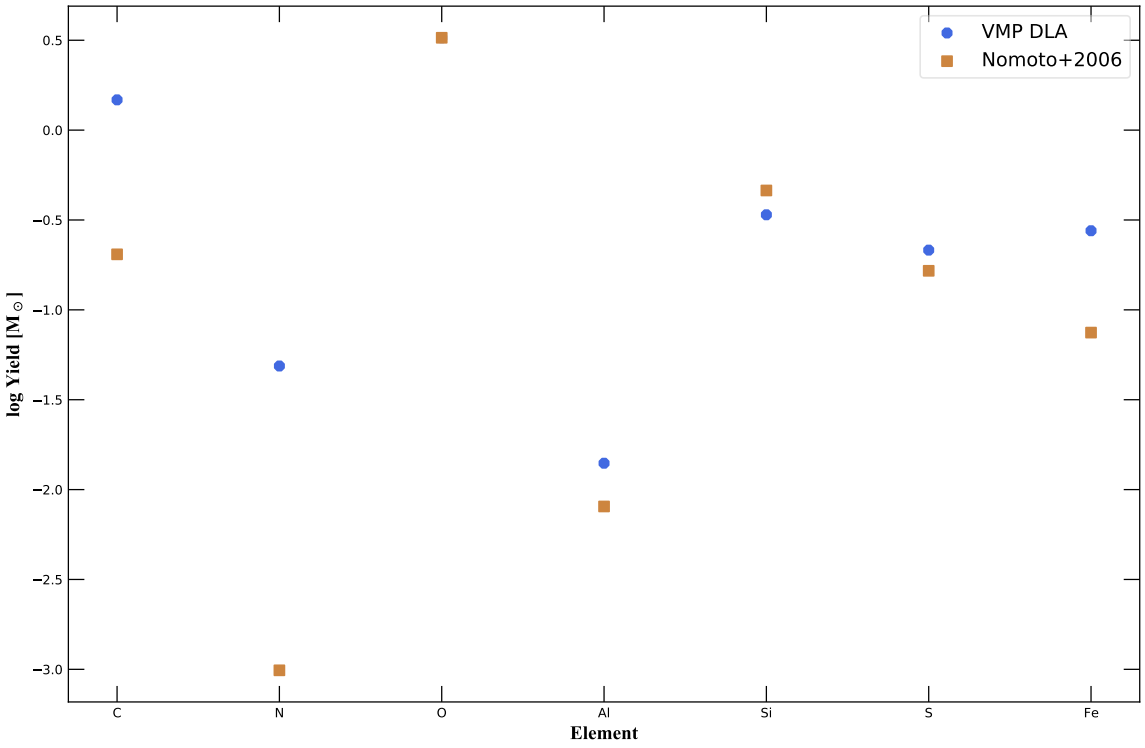

Figure 6. The IMF-averaged yields predictions of theoretical yields and VMP DLA constrained yields. The standard yields from N06 CCSNe yields are shown as orange squares and the VMP DLA constrained yields are shown as blue octagons. O is identical by construction.

where $\overline{M}_{Fe}$ is the VMP DLA constrained IMF averaged Fe yield, $\overline{[X/Fe]}$ is the average VMP DLA abundance ratio for element X, $\log(n_X)_\odot$ is the solar abundance of element X, and m_X is the atomic mass of element X. I can also write this in an alternate form by subbing Equation 1 into Equation 2 resulting in Equation 3 which removes the Fe dependency in the expression by replacing it with Oxygen, the "true" reference element.

$$\overline{M}_X = \overline{M}_O * 10^{(\overline{[X/Fe]} - \overline{[O/Fe]} + \log(n_X)_\odot - \log(n_O)_\odot)} \frac{m_X}{m_O} \tag{3}$$

I computed the IMF-averaged yields for each element, use the previous equations to calculate their the new yield from the VMP DLA constraints, then made a comparison plot showing the resultant yields in Figure 6.

There are differences across the board, except for Oxygen since it is the reference element. The elements that show the smallest difference between the modeled and constrained yields are Silicon and Sulfur at < 0.2 dex, and Al at $\sim$0.3 dex. Fe is in the middle with a difference of $\sim$0.5 dex. Carbon and Nitrogen see the largest difference of $\sim$0.8 dex and $\sim$1.7 dex. Now I will investigate how the constraints would propagate through a galactic chemical evolution model.

4.2. *Galactic Chemical Evolution Model of Sculptor*

I apply the VMP DLA constraints to a galactic chemical evolution (GCE) code called OMEGA to model the abundances ratios present in the dwarf spheroidal galaxy Sculptor. OMEGA, One-zone Model for the Evolution of GAlaxies, is a one-zone GCE Python code that can run three simple models (Côté et al. 2017, hereafter C17). In this work I only use and discuss one model, the Inflow/Outflow (IO) model, since IO is the simplest of the models and has been shown to adequately reproduce the trends in Sculptor with the correct parameter combination (C17).

I note that because of the one-zone nature of OMEGA there are processes that are not accounted for that would affect the behavior of the model such as metal-rich outflows, star-formation thresholds, and gas-stripping (C17). Since I am just interested in the differences between model runs this is not crucial. The main equation that OMEGA solves is shown in Equation 4.

$$M_{gas}(t + \Delta t) = M_{gas}(t) + [\dot{M}_{in}(t) + \dot{M}_{ej}(t) - \dot{M}_*(t) - \dot{M}_{out}(t)]\Delta t \tag{4}$$

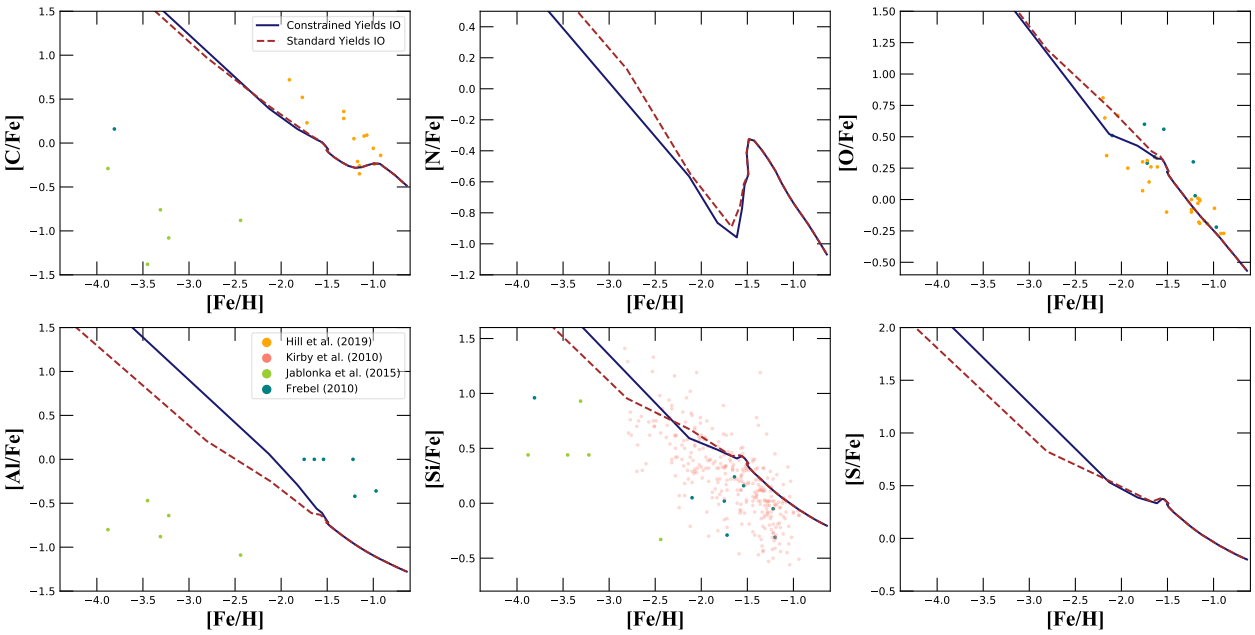

Figure 7. C, N, O, Al, Si, and S modeled abundance ratios using OMEGA in the IO mode. The blue solid lines show the DLA constrained yields and the brown dashed lines show the standard yields. The points are red giant stars in Sculptor; gold from Hill et al. (2019), pink from Kirby et al. (2010), green from Jablonka et al. (2015), and blue from Frebel et al. (2010)

.

where M_{gas} is the gas mass, $\dot{M}_{in}$ is the gas inflow rate, $\dot{M}_{out}$ is the gas outflow rate, and $\dot{M}_{ej}$ is the stellar ejecta rate. The IO mode focuses on the inflow and outflow rate of the galaxy at each timestep. Both quantities are directly proportional to the star formation rate. The outflow rate is shown in Equation 5.

$$\dot{M}_{out}(t) = \eta \dot{M}_{*}(t) \tag{5}$$

where η is the mass-loading parameter, a free parameter. Similarly the inflow rate follows the same form, shown in Equation 6.

$$\dot{M}_{in}(t) = \xi \dot{M}_{*}(t) \tag{6}$$

where ξ is a free parameter that can be linked to the mass-loading parameter.

We adopt the best-fit values of the free parameters for Sculptor that were published by C17. These include constraints on the CCSNe transition mass, number of SNe Ia to explode, and initial mass of Scupltor. I note that when C17 ran their Markov-Chain Monte-Carlo (MCMC) simulation to find these best-fit values, they used nine elements to constrain the model and of those nine, only Si and O are in common with my sample.

I ran OMEGA with the best-fit free parameters twice, once with OMEGAs standard theoretical yield tables and second with the VMP DLA yield constrained yields. Fundamentally this changes the stellar ejecta rate ($\dot{M}_{ej}$ in Equation 4. I show the results of the model runs in Figure 7.

It can be seen in Figure 7 that for all models (except O), that the evolution differs most apparently in the most metal poor regime, [Fe/H] < -2. At higher metallicities, [Fe/H] > -1.5, where the chemical evolution is dominated by SNe Ia, the models converge. The largest differences occur in Al with a difference of ∼0.4 dex whereas the smallest is seen in N due to the small amount of N because it is not produced significantly in either the VMP DLA constrained yields or the theoretical yields. C, Si, and S have similar differences of ∼0.2 dex.

The models only fit the datapoints well for Si and O only due to the aforementioned data constraints that C17 used when developing their best-fit-parameters. I also note that the [α/Fe] plateau should be present in the model but there is a software bug causing the spurious output.

5. FUTURE WORK

The next step(s) in the project would be to expand comparisons to different CCSNe yield tables. This would be in the interest of finding the yields that most closely resemble what the VMP DLAs are informing. Along with that would be running the results through OMEGA again but this time running it through my own MCMC simulation.

There are ongoing observational campaigns to acquire more high-resolution VMP DLA data so getting involved in any of those would be another ideal step. This would increase my overall sample size and increase the population statistics of the abundances of VMP DLAs as a whole.

I would like to thank my fantastic advisor Evan N. Kirby for enlightening discussions and helpful comments throughout the duration of this project; Chuck Steidel for his data suggestions; all of the first year grads, and in particular Samantha C. Wu, for being so pleasant and down to Earth during these times.

REFERENCES

Abohalima, A., & Frebel, A. 2018, ApJS, 238, 36, doi: 10.3847/1538-4365/aadfe9

Asplund, M., Grevesse, N., Sauval, A. J., & Scott, P. 2009, ARA&A, 47, 481, doi: 10.1146/annurev.astro.46.060407.145222

Berg, T. A. M., Ellison, S. L., Sánchez-Ramírez, R., et al. 2016, MNRAS, 463, 3021, doi: 10.1093/mnras/stw2232

Centurión, M., Molaro, P., Vladilo, G., et al. 2003, A&A, 403, 55, doi: 10.1051/0004-6361:20030273

Chiappini, C. 2001, American Scientist, 89, 506, doi: 10.1511/2001.6.506

Chiappini, C., Matteucci, F., & Gratton, R. 1997, ApJ, 477, 765, doi: 10.1086/303726

Cooke, R., Pettini, M., Jorgenson, R. A., et al. 2013, MNRAS, 431, 1625, doi: 10.1093/mnras/stt282

Cooke, R., Pettini, M., & Murphy, M. T. 2012, MNRAS, 425, 347, doi: 10.1111/j.1365-2966.2012.21470.x

Cooke, R., Pettini, M., Steidel, C. C., Rudie, G. C., & Jorgenson, R. A. 2011a, MNRAS, 412, 1047, doi: 10.1111/j.1365-2966.2010.17966.x

Cooke, R., Pettini, M., Steidel, C. C., Rudie, G. C., & Nissen, P. E. 2011b, MNRAS, 417, 1534, doi: 10.1111/j.1365-2966.2011.19365.x

Cooke, R. J., & Madau, P. 2014, ApJ, 791, 116, doi: 10.1088/0004-637X/791/2/116

Cooke, R. J., Pettini, M., & Jorgenson, R. A. 2015, ApJ, 800, 12, doi: 10.1088/0004-637X/800/1/12

Cooke, R. J., Pettini, M., & Steidel, C. C. 2017, MNRAS, 467, 802, doi: 10.1093/mnras/stx037

Côté, B., O'Shea, B. W., Ritter, C., Herwig, F., & Venn, K. A. 2017, ApJ, 835, 128, doi: 10.3847/1538-4357/835/2/128

Côté, B., West, C., Heger, A., et al. 2016, MNRAS, 463, 3755, doi: 10.1093/mnras/stw2244

de los Reyes, M. A. C., Kirby, E. N., Seitenzahl, I. R., & Shen, K. J. 2020, ApJ, 891, 85, doi: 10.3847/1538-4357/ab736f

Dekker, H., D'Odorico, S., Kaufer, A., Delabre, B., & Kotzlowski, H. 2000, in Society of Photo-Optical Instrumentation Engineers (SPIE) Conference Series, Vol. 4008, Optical and IR Telescope Instrumentation and Detectors, ed. M. Iye & A. F. Moorwood, 534–545

Dessauges-Zavadsky, M., D'Odorico, S., McMahon, R. G., et al. 2001, A&A, 370, 426, doi: 10.1051/0004-6361:20010217

Dessauges-Zavadsky, M., Péroux, C., Kim, T. S., D'Odorico, S., & McMahon, R. G. 2003, MNRAS, 345, 447, doi: 10.1046/j.1365-8711.2003.06949.x

D'Odorico, V., Feruglio, C., Ferrara, A., et al. 2018, ApJL, 863, L29, doi: 10.3847/2041-8213/aad7b7

Ellison, S. L., & Lopez, S. 2001, A&A, 380, 117, doi: 10.1051/0004-6361:20011431

Ellison, S. L., Prochaska, J. X., Hennawi, J., et al. 2010, MNRAS, 406, 1435, doi: 10.1111/j.1365-2966.2010.16780.x

Frebel, A., Simon, J. D., Geha, M., & Willman, B. 2010, ApJ, 708, 560, doi: 10.1088/0004-637X/708/1/560

Heger, A., & Woosley, S. E. 2010, ApJ, 724, 341, doi: 10.1088/0004-637X/724/1/341

Hill, V., Skúladóttir, Á., Tolstoy, E., et al. 2019, A&A, 626, A15, doi: 10.1051/0004-6361/201833950

Hopkins, P. F., Wetzel, A., Kereš, D., et al. 2018, MNRAS, 480, 800, doi: 10.1093/mnras/sty1690

Jablonka, P., North, P., Mashonkina, L., et al. 2015, A&A, 583, A67, doi: 10.1051/0004-6361/201525661

Kirby, E. N., Guhathakurta, P., Simon, J. D., et al. 2010, ApJS, 191, 352, doi: 10.1088/0067-0049/191/2/352

Kirby, E. N., Xie, J. L., Guo, R., et al. 2019, ApJ, 881, 45, doi: 10.3847/1538-4357/ab2c02

Levshakov, S. A., Agafonova, I. I., Centurión, M., & Mazets, I. E. 2002, A&A, 383, 813, doi: 10.1051/0004-6361:20011807

Lopez, S., Reimers, D., D'Odorico, S., & Prochaska, J. X. 2002, A&A, 385, 778, doi: 10.1051/0004-6361:20020181

Lu, L., Sargent, W. L. W., & Barlow, T. A. 1998, AJ, 115, 55, doi: 10.1086/300180

Molaro, P., Bonifacio, P., Centurión, M., et al. 2000, ApJ, 541, 54, doi: 10.1086/309439

Molaro, P., Levshakov, S. A., D'Odorico, S., Bonifacio, P., & Centurión, M. 2001, ApJ, 549, 90, doi: 10.1086/319072

Nomoto, K., Tominaga, N., Umeda, H., Kobayashi, C., & Maeda, K. 2006, NuPhA, 777, 424, doi: 10.1016/j.nuclphysa.2006.05.008

Penprase, B. E., Prochaska, J. X., Sargent, W. L. W., Toro-Martinez, I., & Beeler, D. J. 2010, ApJ, 721, 1, doi: 10.1088/0004-637X/721/1/1

Petitjean, P., Ledoux, C., & Srianand, R. 2008, A&A, 480, 349, doi: 10.1051/0004-6361:20078607

Pettini, M. 2011, Proceedings of the Royal Society of London Series A, 467, 2735, doi: 10.1098/rspa.2011.0117

Pettini, M., Ellison, S. L., Bergeron, J., & Petitjean, P. 2002, A&A, 391, 21, doi: 10.1051/0004-6361:20020809

Pettini, M., Zych, B. J., Steidel, C. C., & Chaffee, F. H. 2008, MNRAS, 385, 2011, doi: 10.1111/j.1365-2966.2008.12951.x

Prochaska, J. X., & Wolfe, A. M. 2002, ApJ, 566, 68, doi: 10.1086/338080

Prochaska, J. X., Wolfe, A. M., Howk, J. C., et al. 2007, ApJS, 171, 29, doi: 10.1086/513714

Prochaska, J. X., Wolfe, A. M., Tytler, D., et al. 2001, ApJS, 137, 21, doi: 10.1086/322542

Richards, G. T., Fan, X., Newberg, H. J., et al. 2002, AJ, 123, 2945, doi: 10.1086/340187

Romano, D., Karakas, A. I., Tosi, M., & Matteucci, F. 2010, A&A, 522, A32, doi: 10.1051/0004-6361/201014483

Sheinis, A. I., Bolte, M., Epps, H. W., et al. 2002, PASP, 114, 851, doi: 10.1086/341706

Srianand, R., Gupta, N., Petitjean, P., Noterdaeme, P., & Ledoux, C. 2010, MNRAS, 405, 1888, doi: 10.1111/j.1365-2966.2010.16574.x

Vogt, S. S., Allen, S. L., Bigelow, B. C., et al. 1994, in Society of Photo-Optical Instrumentation Engineers (SPIE) Conference Series, Vol. 2198, Instrumentation in Astronomy VIII, ed. D. L. Crawford & E. R. Craine, 362

Welsh, L., Cooke, R., & Fumagalli, M. 2019, MNRAS, 487, 3363, doi: 10.1093/mnras/stz1526

Welsh, L., Cooke, R., Fumagalli, M., & Pettini, M. 2020, MNRAS, 494, 1411, doi: 10.1093/mnras/staa807

Wolfe, A. M., Gawiser, E., & Prochaska, J. X. 2005, ARA&A, 43, 861, doi: 10.1146/annurev.astro.42.053102.133950

Wolfe, A. M., Turnshek, D. A., Smith, H. E., & Cohen, R. D. 1986, ApJS, 61, 249, doi: 10.1086/191114

Woosley, S. E., Heger, A., & Weaver, T. A. 2002, Reviews of Modern Physics, 74, 1015, doi: 10.1103/RevModPhys.74.1015

Woosley, S. E., & Weaver, T. A. 1995, ApJS, 101, 181, doi: 10.1086/192237

Zafar, T., Vladilo, G., Péroux, C., et al. 2014, MNRAS, 445, 2093, doi: 10.1093/mnras/stu1904